



# Vibrational mode and sound radiation of electrostatic speakers using circular and annular diaphragms



Yu-Hsi Huang\*, Hsin-Yuan Chiang

Department of Mechanical Engineering, National Taiwan University of Science and Technology, No. 43, Section 4, Keelung Rd., Taipei 10607, Taiwan, ROC

## ARTICLE INFO

### Article history:

Received 6 October 2015

Received in revised form

21 January 2016

Accepted 8 February 2016

Handling Editor: P. Joseph

Available online 28 February 2016

### Keywords:

Vibrational mode

Sound

Electrostatic speaker

Diaphragm

## ABSTRACT

This study modeled two diaphragms comprising a pair of indium tin oxide (ITO) transparent plates sandwiching a vibrating diaphragm to create circular (30 mm radius) and annular (30 mm outer and 3 mm inner radius) push–pull electrostatic speakers. We then measured the displacement amplitudes and mode shapes produced by the devices. Vibration characteristics were used to predict sound pressure levels (SPLs) using the lumped parameter method (LPM) and distributed parameter method (DPM). The two measurement results obtained using a laser system were compared to the SPLs obtained using traditional acoustic measurement (AM) from 20 Hz to 20 kHz in order to verify our predictions. When using LPM and DPM, the SPL prediction results in the first three symmetric modes were in good agreement with the AM results. Under the assumption of linear operations, the DPM and amplitude-fluctuation electronic speckle pattern interferometry (ESPI) techniques proved effective in determining the visualization of mode shape (0,1)–(0,3). The use of ITO plates is a practical technique for the prediction of SPL, as well as measurement of mode shapes. The four evaluation methods, i.e. LPM, DPM, ESPI and AM, present a high degree of consistency with regard to vibrational mode and sound radiation characteristics.

© 2016 Elsevier Ltd. All rights reserved.

## 1. Introduction

Membranes have many applications in acoustics. Membrane surfaces (i.e., vibrating diaphragms) are a fundamental component of speakers, microphones, and musical instruments (e.g., drums). Speakers and microphones are the most common sound actuators and sensors and are, in fact, closely related. Different drive mechanisms, such as dynamic moving-coil, electrostatic, and piezoelectric types, result in different vibration and sound characteristics. Electrostatic headphones and loudspeakers produce sound of very high fidelity with low distortion [1,2]. Push–pull electrostatic speakers comprise a sandwich of two conductive plates fashioned with a two-dimensional (2D) array of holes. A thin diaphragm (membrane) is suspended between the two conductive plates. The diaphragm material must be able to hold a charge of direct current (DC) bias voltage, such that the subsequent application of alternating current (AC) to the conductive plates produces a uniform electrostatic field proportional to the source audio signal. This creates a push–pull force acting on the diaphragm, the movement of which acts on the surrounding air to produce an audible signal.

\* Corresponding author.

E-mail address: [yhhuang@mail.ntust.edu.tw](mailto:yhhuang@mail.ntust.edu.tw) (Y.-H. Huang).

The construction of electrostatic earphones and loudspeakers was described by Selsted [1] and Sanders [3], respectively. Compared to single-ended speakers, push-pull electrostatic speakers provide a diaphragm with greater stability, which reduces second-order distortion. In the 1960s and 1970s, several researchers [4–6] designed electrostatic headphones and amplifiers. They determined that the conductive plates of electrostatic speakers must be rigid and provide an opening of least 20%. To achieve maximum acoustic output, the thickness of the spacer should be as small as possible (0.37–0.8 mm) without restricting the movement of the diaphragm at low frequencies. Diaphragms are generally thin and flexible (thickness of less than  $15 \times 10^{-3}$  mm) and made from polymer films capable of holding a charge generated from a DC bias voltage. These pioneers also outlined the fundamentals of electrostatic speaker constructions as, well as the characteristic responses in the open air and with artificial ears.

The vibration characteristics of circular membranes have been discussed in numerous papers. Membranes have far more freedom with regard to vibration than do strings. The careful selection of polar coordinates for the circular boundary can help to overcome many of the problems associated with circular membranes [7]. Sharp [8] presented a finite transform solution for annular membranes with symmetrical vibration characteristics using completely arbitrary initial and boundary conditions. Jabareen and Eisenberger [9] provided exact solutions for axisymmetric as well as antisymmetric modes of circular and annular membranes wherein, any piecewise polynomial variation in density can be obtained using a power series solution. They solved dynamic problems using the dynamic stiffness method for circular and annular membrane elements. Streng [10,11] calculated the membrane deflection and sound-field characteristics of electrostatic push-pull loudspeakers based on circular stretched-membranes in free space. Mellow and Kärkkäinen [12] presented an enhanced method for calculating the radiation characteristics of circular membranes in free space and in an infinite baffle.

There have been several recent reports on new materials and manufacturing methods used in the fabrication of electrostatic speakers. Bai et al. [13] conducted electroacoustic analysis of a single-ended electret loudspeaker combining finite-element and lumped-parameter models. Experimental results revealed that the single-ended electret loudspeaker suffered from a high degree of nonlinear distortion. They later [14] presented a full experimental modeling technique and design optimization procedures applicable to push-pull electret loudspeakers. The diaphragm they employed was made of fluoropolymer with nanopores to enhance charge density and stability. The push-pull configuration effectively overcomes the problem of nonlinearity found in the single-ended configuration. Zhou and Zettl [15] used a graphene diaphragm, 7 mm in diameter with a DC bias voltage of 100 V, as an audio transducer (earphone) based on the push-pull electrostatic principle. They also described sound pressure levels (SPLs) over the relevant audio frequency range using graphene speakers and high-quality commercial earphones. Chiang and Huang [16] employed the lumped parameter method (LPM) and distributed parameter method (DPM) in the measurement of vibration and the prediction of sound pressure in push-pull electrostatic speakers. The electrostatic speaker was fabricated by suspending a circular diaphragm (60 mm diameter) between two indium tin oxide (ITO) plates. The SPL values predicted using LPM and DPM were identical to those obtained via acoustic measurement. Huang et al. [17] illustrated transverse and planar vibration characteristics in two-layered piezoceramic disks in order to determine the traction-free boundary conditions using theoretical and finite element analysis as well as experimental measurements. Amplitude-fluctuation electronic speckle pattern interferometry (ESPI), laser Doppler vibrometer (LDV), and impedance analysis were used to take measurements and verify the theoretical solutions to transverse and extensional vibrations.

In this study, we employed metal sputtering on a polymer film (low mass) in the fabrication of a push-pull electrostatic speaker. This is a relatively inexpensive, facile, and, yet, a reliable process. We employed semi-analytical as well as experimental methods to predict SPL values in order to avoid the inaccuracies that inevitably occur when using the approach of finite element analysis for modeling based on uncertain properties (e.g., uniform pressure difference, specific acoustic impedance, and tension in the diaphragm). This study had three objectives. First, we sought to develop push-pull electrostatic speakers using transparent ITO plates to overcome the vibrational measurement. Second, we developed a rapid yet accurate technique for the experimental measurement of vibrations and the prediction of sound pressure without resorting to a sound field (e.g., in an anechoic chamber). Third, on the basis of the circular diaphragm, we developed [16], aiming at modeling the annular diaphragm to measure the displacement amplitudes and mode shapes, and to predict the SPLs.

The experimental used methods in this study are as follows: (1) LPM for the measurement of displacement amplitudes and prediction of modes and SPLs; (2) DPM for the measurement of mode shapes and the prediction of SPLs; (3) amplitude-fluctuation ESPI for the measurement of mode shapes (fringe patterns); and (4) acoustic measurement (AM) for the measurement of SPLs in a sound field. The experimental results demonstrate that the predicted modes and SPLs are in good agreement with the measured mode shapes and SPLs in ITO electrostatic speakers based on circular and annular diaphragms. The use of ITO plates is a practical technique for measuring mode shapes and predicting SPLs. This approach could be applied to a variety of thin-film speakers and microphones that employ perforated sheets.

## 2. Experiments: materials and methods

Without additional damping provided by a woven mesh with acoustic airflow resistance, the thin, light diaphragm found in electrostatic speakers vibrates in many resonant modes with many peaks in the displacement amplitude. To investigate the frequency-response characteristics associated with vibrational modes and sound pressure, we employed LPM, DPM and

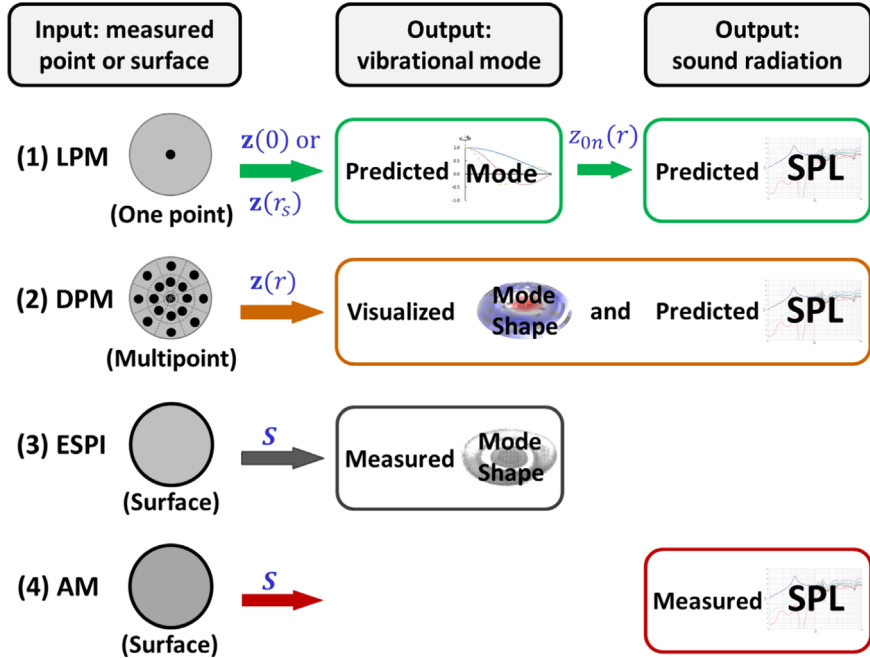


Fig. 1. Flowchart showing inputs and outputs used in measurement of vibrational mode and sound radiation using LPM, DPM, ESPI and AM.

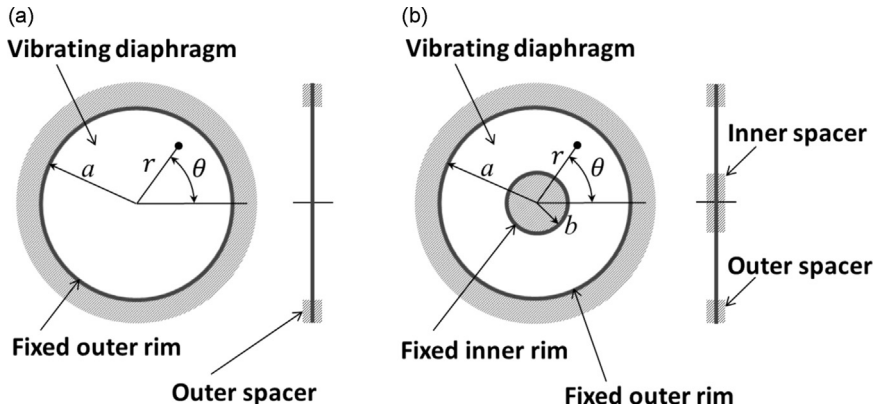


Fig. 2. Geometry and polar coordinates: (a) circular diaphragm with fixed outer rim, and (b) annular diaphragm with fixed outer and inner rims.

ESPI to process the data obtained from laser scanning systems. Then, the electrostatic speakers were fixed to a baffle in an anechoic chamber to obtain SPL curves for further comparison. Fig. 1 presents a flowchart outlining the process used to determine vibrational modes and SPL values using the four methods.

## 2.1. Construction of push-pull electrostatic speakers

Our design of electrostatic speakers is similar to that used in [3–6], based on the constant charge push–pull principle provided by a DC bias voltage. This study employed electrostatic speakers with two types of diaphragm: (1) a circular diaphragm (outer radius  $a=30$  mm) and (2) an annular diaphragm (outer radius  $a=30$  mm, and inner radius  $b=3$  mm), as illustrated in Fig. 2. The electrostatic speaker with a circular diaphragm comprises two ITO plates, two outer spacers, and one diaphragm. The electrostatic speaker with an annular diaphragm comprises two ITO plates, two outer and inner spacers, and one diaphragm. The components are illustrated in Fig. 3.

We cut conductive plates of ITO glass (0.7 mm thickness) and then produced a 2D array by drilling holes using a UV laser fabrication process. After deburring the holes ( $radius\ a_h=0.65$  mm), the resulting spaces accounted for 33.2% of the plate area. Spacers were cut from a single sheet of 0.5 mm-thick polycarbonate, which is an excellent insulator with uniform thickness. The gap between the ITO plate and diaphragm is  $d=0.5$  mm, and the maximum displacement amplitude of the vibrating diaphragm must be less than the gap distance. The diaphragm is made from polymer film (thickness

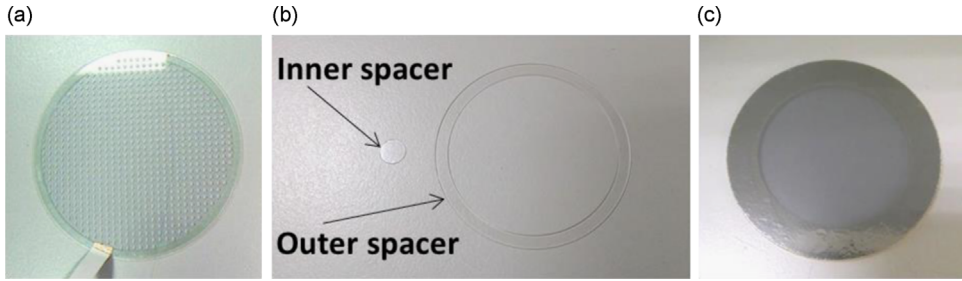


**Fig. 3.** Components used in electrostatic speakers: (a) transparent ITO plate, (b) outer and inner spacers, and (c) vibrating diaphragm.

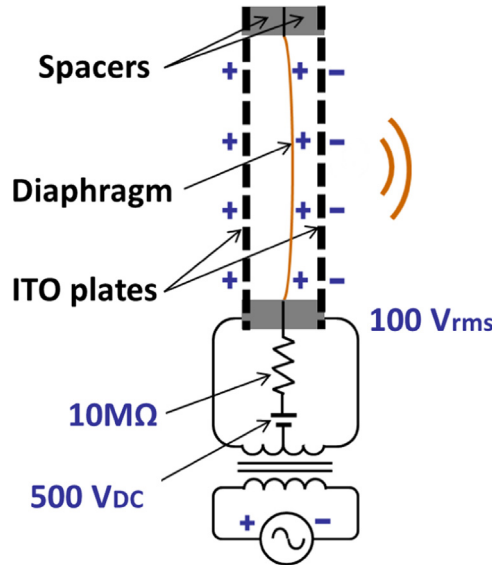


**Fig. 4.** Schematic diagram and operating principle of push-pull electrostatic speaker based on ITO plates.

$h=2 \times 10^{-3}$  mm, and mass density  $\rho_v=1340$  kg/m<sup>3</sup>) coated on one side with nickel, and uniformly stretched and attached to a supporting frame.

The two ITO plates and vibrating diaphragm are sandwiched together to assemble the push-pull electrostatic speakers (either circular or annular). As shown in Fig. 4, the boundary conditions of both electrostatic speaker designs are restricted by the dimensions of the spacers between the ITO plates and diaphragm. To test the speakers, the vibrating diaphragm was supplied a constant charge by a DC bias voltage measuring  $E_b=500$  V with a 10 MΩ resistor. The two conductive ITO plates were driven by an AC audio signal of  $E_a=100$  V<sub>rms</sub>. In linear motion, the uniform electrostatic field is proportional to the AC signal between the two conductive plates. We then measured the vibration and sound generated by the speakers in the audible frequency band. The experimental parameters used in the study are listed in Table 1.

## 2.2. Lumped parameter method (LPM)

Fig. 2(a) presents a circular diaphragm with fixed outer rim ( $r=a$ ) and an associated polar coordinate ( $r, \theta$ ), and Fig. 2(b) presents an annular diaphragm with fixed outer rim ( $r=a$ ) and inner rim ( $r=b$ ). In linear operations, LPM can be used to measure the displacement amplitude  $z$  at the center of a circular diaphragm, or at a specified point on an annular diaphragm, to enable the prediction of vibrational modes using the Helmholtz equation and sound pressure using the Rayleigh integral equation.

The wave equation of a diaphragm is very similar to that of a string. Consider a stretched diaphragm with a fixed rim subjected to uniform tension  $T$  (N/m) and undergoing free, undamped vibration. We can obtain the classical, two-dimensional wave equation in the general Laplacian form as follows:

$$T\nabla^2 z = \rho_v h \frac{\partial^2 z}{\partial t^2} \quad (1)$$

**Table 1**

Parameters of electrostatic speakers with circular and annular diaphragm.

Parameter	Value
Outer radius of circular and annular diaphragm, $a$ (mm)	30
Inner radius of annular diaphragm, $b$ (mm)	3
Thickness of diaphragm, $h$ (mm)	$2 \times 10^{-3}$
Mass density of diaphragm, $\rho_v$ ( $\text{kg}/\text{m}^3$ )	1340
Hole radius of ITO plate, $d_h$ (mm)	0.65
Distance from ITO plate to diaphragm, $d$ (mm)	0.5
Density of air, $\rho_0$ ( $\text{kg}/\text{m}^3$ )	1.18
Distance along z-axis in the sound field, $r_z$ (m)	0.1
AC audio signal (rms), $E_a$ (V)	100
DC bias voltage, $E_b$ (V)	500

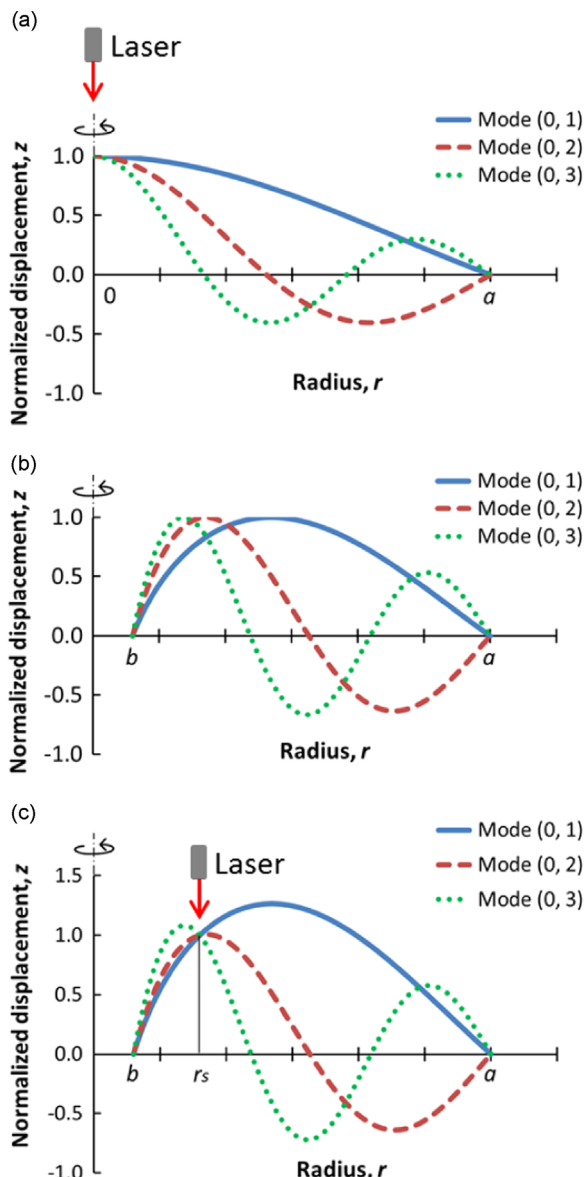


**Fig. 5.** Normalized displacement amplitudes of modes (0,1)–(0,3) obtained using LPM: (a) circular diaphragm with normalized point at  $r=0$ , (b) annular diaphragm with normalized point at maximum displacement amplitude of each mode, and (c) annular diaphragm with normalized point at  $r=r_s$ ,  $b < r_s < a$ .

where  $z$  (m) is the displacement amplitude of the diaphragm,  $\rho_v$  ( $\text{kg}/\text{m}^3$ ) is the mass density of the diaphragm, and  $h$  (m) is the thickness of the diaphragm. For a circular diaphragm fixed at  $r=a$ , the Laplacian is

$$\nabla^2 = \frac{\partial^2}{\partial r^2} + \frac{1}{r} \frac{\partial}{\partial r} + \frac{1}{r^2} \frac{\partial^2}{\partial \theta^2} \quad (2)$$

in polar coordinates.

Suppose that the motion is harmonic at angular velocity  $\omega$ , then assuming a separable solution:

$$\mathbf{z}(r, \theta, t) = \Psi e^{j\omega t} \quad (3)$$

where  $\Psi = \mathbf{R}(r)\Theta(\theta)$  is a function only of position, and the symbols in boldface type represent complex numbers; substitution into Eq. (1) yields the time-independent Helmholtz equation

$$\nabla^2 \Psi + k_d^2 \Psi = 0 \quad (4)$$

where the wavenumber in the diaphragm is  $k_d = \omega/c_d$ , in which  $c_d$  is the velocity of the transverse wave in the diaphragm relative to  $c_d^2 = T/\rho_v h$ . Using Eq. (2) in Eq. (4) yields

$$\frac{d^2 \mathbf{R}}{dr^2} + \frac{1}{r} \frac{d\mathbf{R}}{dr} + \frac{\mathbf{R}}{r^2} \frac{d^2 \Theta}{d\theta^2} + k_d^2 \mathbf{R}\Theta = 0. \quad (5)$$

The solutions are as follows:

$$\Psi = R\Theta = [\mathbf{A}J_m(k_{dm}r) + \mathbf{B}Y_m(k_{dm}r)] \cos(m\theta + \phi_m) \quad (6)$$

where  $\mathbf{A}$  and  $\mathbf{B}$  are complex constants,  $J_m(k_{dm}r)$  and  $Y_m(k_{dm}r)$  are Bessel functions of the first and second kinds, respectively, of order  $m$  ( $m=0, 1, 2, \dots$ ), and the arbitrary constant  $\phi_m$  is an azimuthal phase angle.

The situation involving symmetric vibrations (i.e.,  $m=0$ ) from a circular or annular diaphragm fixed at the rim holds considerable interest for us. The first several symmetric modes are useful for predicting sound pressure.

As shown in Fig. 2(a), in the case of a circular diaphragm ( $0 \leq r \leq a$ ), because of the boundary conditions,  $\mathbf{R}(a)=0$ , and because  $\mathbf{R}(0)$  has a finite value, we can reduce Eq. (6) to

$$\mathbf{z}_{0n}(r)_{\text{cir}} = \mathbf{A}_{0n}J_0(k_{d0n}r) = \mathbf{A}_{0n}J_0\left(\frac{j_{0n}}{a}r\right) \quad (7)$$

where  $J_0(k_{d0n}r)$  is a Bessel function of the first kind of order zero,  $k_d$  assumes the discrete values  $k_{d0n}a=j_{0n}$ , and  $j_{01}=2.405$ ,  $j_{02}=5.520$ ,  $j_{03}=8.654, \dots$ . Fig. 5(a) presents the normalized displacements at the center of the first three symmetric modes of the circular diaphragm. LPM makes it possible to measure the displacement amplitudes of vibrating diaphragms using laser displacement sensor or LDV. This approach enables non-contact measurement and a facile means of obtaining the absolute or relative displacement. In this study, we used a laser displacement sensor (Keyence LK-H052, Osaka, Japan) of KLIPPEL R&D System (Klippel GmbH, Dresden, Germany) for the measurement of displacement amplitudes at the center ( $r=0$ ) of the circular diaphragm, as it pertains to frequency response ( $f$ ), such that Eq. (7) can be written as

$$z_{0n}(r, f)_{\text{cir}} = A_c(f)J_0\left(\frac{j_{0n}}{a}r\right) \quad (8)$$

where  $z_{0n}(r, f)_{\text{cir}}$  is the predicted displacement amplitude of the  $n$ th symmetric mode on the circular diaphragm, and  $A_c$  is the measured displacement amplitude at the center of the circular diaphragm.

As shown in Fig. 2(b), in the case of an annular diaphragm between inner and outer rims ( $b \leq r \leq a$ ), applying the boundary conditions  $\mathbf{R}(a)=0$  and  $\mathbf{R}(b)=0$  yields

$$\begin{bmatrix} J_0(k_{d0n}a) & Y_0(k_{d0n}a) \\ J_0(k_{d0n}b) & Y_0(k_{d0n}b) \end{bmatrix} \begin{bmatrix} \mathbf{A}_{0n} \\ \mathbf{B}_{0n} \end{bmatrix} = \begin{bmatrix} 0 \\ 0 \end{bmatrix}. \quad (9)$$

To obtain a nontrivial solution, the determinant of the coefficient matrix in Eq. (9) is set to zero, i.e.,

$$J_0(\lambda_{0n})Y_0\left(\frac{b}{a}\lambda_{0n}\right) - J_0\left(\frac{b}{a}\lambda_{0n}\right)Y_0(\lambda_{0n}) = 0 \quad (10)$$

where  $b/a < 1$  and  $\lambda_{0n}=k_{d0n}a$ . For any given value of  $b/a$ , symmetric mode frequencies of the annular diaphragm can be obtained using Eq. (10). For example, if  $b/a=0.1$ , then the first few roots (non-dimensional frequencies) [18] will be  $\lambda_{01}=3.314$ ,  $\lambda_{02}=6.858$ ,  $\lambda_{03}=10.377, \dots$ . The solutions of Eq. (6) can be expressed as

$$\mathbf{z}_{0n}(r)_{\text{ann}} = \mathbf{A}_{0n}J_0\left(\frac{\lambda_{0n}}{a}r\right) + \mathbf{B}_{0n}Y_0\left(\frac{\lambda_{0n}}{a}r\right) \quad (11)$$

where  $b \leq r \leq a$ . Fig. 5(b) shows the normalized displacement of the first three symmetric modes of the annular diaphragm at the absolute maximum of each mode. Similarly, using the scanning vibrometer to measure the displacement amplitude at

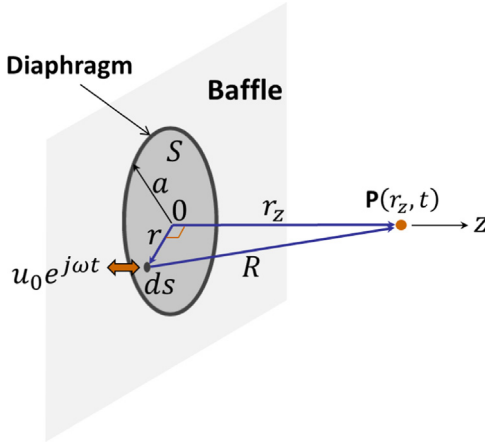


**Fig. 6.** Geometry and coordinates of vibrating diaphragm in half-space sound field.

a specified point ( $b < r_s < a$ ) on the annular diaphragm, Eq. (11) can be written as

$$z_{0n}(r, f)_{\text{ann}} = A_s(f) \left\{ \frac{1}{z_{0n}(r_s)} \left[ A_{0n} J_0 \left( \frac{\lambda_{0n}}{a} r \right) + B_{0n} Y_0 \left( \frac{\lambda_{0n}}{a} r \right) \right] \right\} \quad (12)$$

where  $z_{0n}(r, f)_{\text{ann}}$  is the predicted displacement amplitude of  $n$ th symmetric mode on the annular diaphragm,  $A_s$  is the measured displacement amplitude at the specified point ( $r=r_s$ ) of the annular diaphragm, the item of  $\{ \}$  is the normalized displacement at the specified point of  $n$ th symmetric mode on the annular diaphragm, and  $z_{0n}(r_s) \neq 0$ . For the first three symmetric modes of the annular diaphragm, Fig. 5(c) presents the normalized displacements at the specified points [e.g., in the vicinity between the maximum displacements of modes (0,2) and (0,3)]. Thus, Eqs. (8) and (12) present measured solutions of the Helmholtz equation for the symmetric modes used to calculate the displacement amplitude of surface elements, which are useful for the prediction of sound pressure.

In the evaluation of SPL values, suppose a similar piston of radius  $a$  is fixed on a flat, rigid, infinite baffle. An elemental surface ( $dS$ ) of the piston moves with velocity  $u_0 e^{j\omega t}$  normal to the baffle. The surface is taken as the plane of  $z=0$ . The geometry and coordinates are outlined in Fig. 6. In the sound field, the Rayleigh integral equation [19,20] can be used to calculate the sound pressure along the  $z$ -axis as follows:

$$\mathbf{p}(r_z, t) = \frac{j\omega\rho_0}{2\pi} \iint u_0 e^{j\omega t} \frac{e^{-jkR}}{R} dS \quad (13)$$

where  $r_z$  is the distance of the observation point along the  $z$ -axis, and  $R$  is the distance from each surface element  $dS$  to the observation point. Here, the density of air  $\rho_0$  is  $1.18 \text{ kg/m}^3$ . Considering only the symmetric modes of Eqs. (8) and (12), the total pressure amplitude,  $p$ , at distance  $r_z$  can be written as

$$p(r_z, f) = -\rho_0 (2\pi f)^2 \int_0^a \frac{z_{0n}(r, f)}{\sqrt{r_z^2 + r^2}} r dr \quad (14)$$

for the circular and annular diaphragms of radius  $r \leq a$ . Thus, the measured effective (root-mean-squared) pressure amplitude can be obtained as follows:

$$p_e = \frac{|p(r_z, f)|}{\sqrt{2}}. \quad (15)$$

The minimum audible sound is used as a reference for the sound pressure level (SPL) in decibels (dB). The SPL is calculated using the following:

$$\text{SPL} = 20 \log \left( \frac{p_e}{p_{\text{ref}}} \right) \quad (16)$$

where the reference effective pressure amplitude is  $p_{\text{ref}} = 2 \times 10^{-5} \text{ (Pa)}$ .

Thus, LPM analysis is performed using only one scanning point at the center of the circular diaphragm and at a specified point on the annular diaphragm, plotting the displacement amplitudes and first three symmetric modes are plotted, and then SPL curves at  $r_z=0.1 \text{ m}$  in the half-space sound field are predicted.

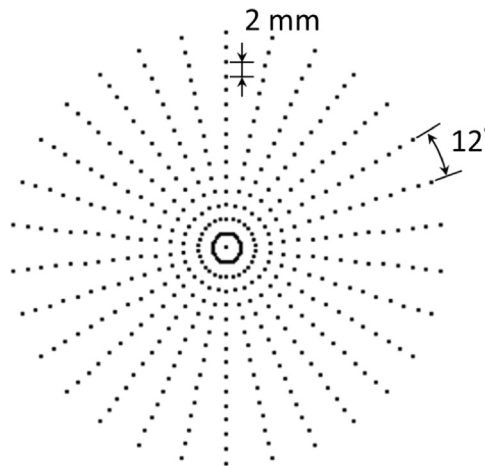


**Fig. 7.** Distribution of 451 scanning points across the circular and annular diaphragms.

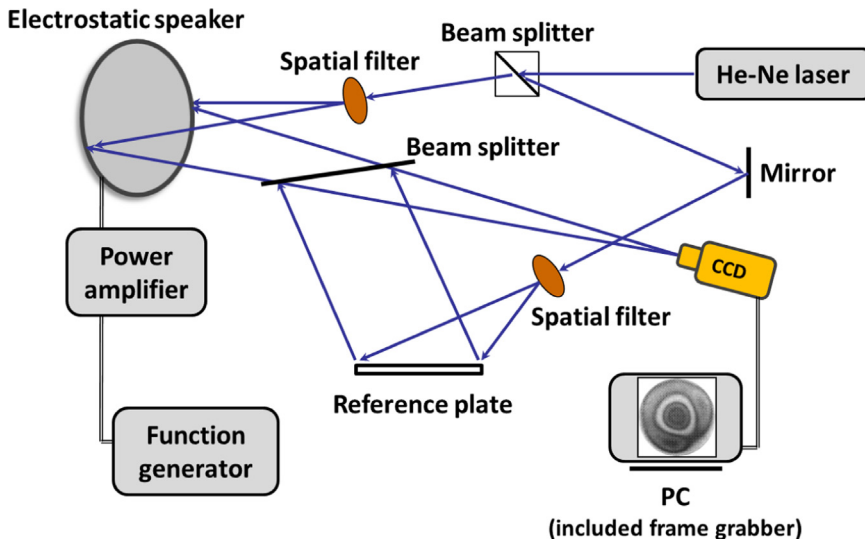


**Fig. 8.** Optical setup of AF-ESPI for measurement of out-of-plane (transverse) vibrations.

### 2.3. Distributed parameter method (DPM)

In linear operations, DPM can be used to measure displacement amplitudes (multipoint measurement) across the entire surface of a circular or annular diaphragm. The measured data can reveal the vibrational modes and predict the sound pressure and related components.

A scanning vibrometer of KLIPPEL R&D System was used to enable the non-contact measurement of mechanical vibration in the diaphragms. SCN is used specifically for loudspeakers, headphones, and other electro-acoustical transducers. It can be described using a set of linear transfer functions with geometric data measured at selected points on the diaphragm using laser triangulation [21]. In this study, SCN hardware comprised a mechanical scanning system with motor control to record the displacement amplitude and phase at each point. Built-in SCN analysis software enables the visualization of mechanical vibration and the prediction of sound pressure in a half-space sound field (i.e., in an infinite baffle) from 20 Hz to 20 kHz. Sound pressure is still determined using Rayleigh integral and boundary-element analysis. The sound pressure decomposition technique [21] reveals that the total mechanical vibration is split into in-phase, anti-phase, and quadrature components, each of which makes a different contribution to SPL output. The in-phase component is a constructive contribution generating the highest SPL. The anti-phase component is a destructive contribution, which reduces SPL. The quadrature component produces positive as well as negative volume velocities, which cancel out in the near field, such that it has no effect on SPL.

In this study, vibration analysis was performed using 451 scanning points across the entire circular and annular diaphragms (see Fig. 7), for the prediction of SPL curves at  $r_z=0.1$  m in the half-space sound field, and to show the mode shapes and position of nodes.

## 2.4. Amplitude-fluctuation electronic speckle pattern interferometry (ESPI)

ESPI is used to determine the resonant frequencies and corresponding mode shapes as well as to present fringe patterns. The ESPI optical technique [22] is a full-field, non-contact, real-time measurement method. Using this method enables the measurement of displacement amplitudes on dynamically vibrating diaphragms in real time from out-of-plane and in-plane setups. It uses a time-average method to obtain the displacement amplitude of a diaphragm in motion within the period of a single photographic frame. Furthermore, the resonant frequency and corresponding mode shape can be measured simultaneously using this kind of optical system.

[Fig. 8](#) illustrates the self-arranged optical setup for measuring out-of-plane (transverse) vibration. A 25 mW He-Ne laser (25 LHP 928, Melles Griot, Carlsbad, CA, USA) with a wavelength of  $\lambda=0.632 \mu\text{m}$  was used as a coherent light source. A beam splitter was used to split the laser beam into two parts, which then passed through spatial filters. For out-of-plane measurement, one laser beam (the object beam) was directed toward the diaphragm of the electrostatic speaker while the other (the reference beam) was used to illuminate the reference plate. When the diaphragm vibrated at a specific frequency, digital images were recorded using a charge-coupled device (CCD, AVTCA203, Allied Vision Technologies, Suite 502 Exton, PA, USA) and speckle fringe patterns were displayed on the monitor in real time. The fringe patterns can be viewed as contours of constant displacement amplitude. The relationship between the intensity of light in the image patterns obtained by ESPI and the displacement amplitude of out-of-plane vibration [17] can be expressed as

$$I \propto |J_0(\Gamma A)| \quad (17)$$

where

$$\Gamma = \frac{2\pi(1 + \cos\theta)}{\lambda} \quad (18)$$

in which  $A$  is the displacement amplitude of out-of-plane vibration, and  $\theta$  is the angle between the object beam and the direction of observation. The related displacement amplitudes  $A_i$ ,  $i=1, 2, 3, \dots$ , for the  $i$ th dark (bright) fringe in the mode shapes can be calculated according to the roots of  $J_0(\Gamma A_i)=0$  for out-of-plane vibration.

We used the angle of optical measurement  $\theta=17^\circ$  for the measurement of out-of-plane vibration. The displacement amplitudes used for the measurement of out-of-plane vibrations associated with the first six dark (bright) fringes were  $A_i=0.124, 0.284, 0.446, 0.607, 0.769$  and  $0.930 \mu\text{m}$  ( $0, 0.197, 0.361, 0.524, 0.686$  and  $0.848 \mu\text{m}$ ), where  $i=1-6$ . The nodal line or circle, which is the zero displacement amplitude, corresponds to the brightest fringe. The displacement amplitudes obtained using ESPI can be evaluated by counting the number of fringes.

In the above experiment, some laser sensors require that the surface of the diaphragm be treated with white paint to generate a diffuse reflection to reduce optical errors. Nonetheless, the white paint must be thin enough not have a noticeable effect on vibration behavior.

## 2.5. Acoustic measurement (AM)

As shown in [Fig. 6](#), we fixed the electrostatic speaker to a baffle at a distance  $r_z=0.1 \text{ m}$  (from speaker to microphone) in an anechoic chamber to compare the predicted SPL values obtained using LPM and DPM. The test was performed at a normal ambient temperature of  $25 \pm 5^\circ\text{C}$  and relative humidity between 30% and 70%. The output SPLs were determined using a 4191 1/2-inch free-field microphone (Brüel & Kjær Sound & Vibration Measurement A/S., Nærum, Denmark) in conjunction with SoundCheck software (Listen Inc., MA, USA).

Our aim was to achieve a frequency response spanning the entire audible frequency band from 20 Hz to 20 kHz. The traditional telephone band generally ranges from about 300 Hz to 3 kHz. As shown in [Fig. 9](#), the audio band can be divided into three sub-bands, each of which has different characteristics. The low-frequency band (bass band) is  $< 500 \text{ Hz}$ , the mid-frequency band (speech band) is from 500 Hz to 3 kHz [23], and the high-frequency band (tweeter band) is  $> 3 \text{ kHz}$ . These audio bands are useful for discussing the frequency response of the speakers.

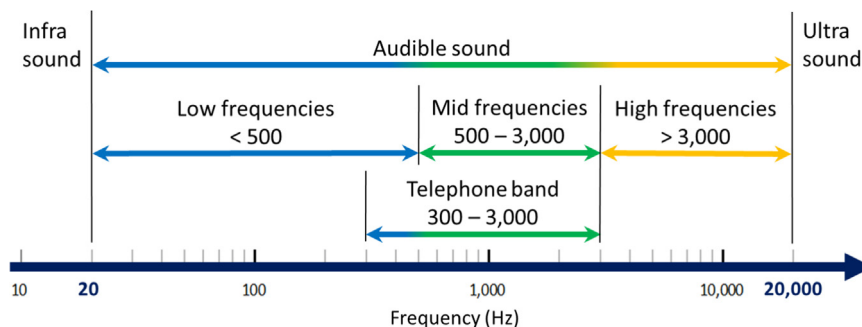


**Fig. 9.** Basic frequency characteristics in audio sub-bands.

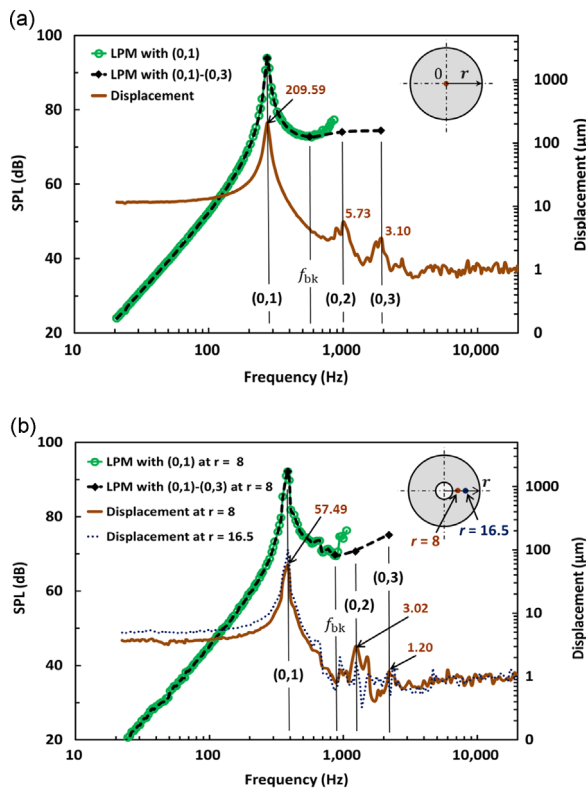


**Fig. 10.** Displacement amplitudes and SPL curves obtained using LPM: electrostatic speakers with (a) circular, and (b) annular diaphragms.

### 3. Results and discussion

In this study, we applied the same tension to the circular and annular diaphragms. Experimental results on the vibrational modes and SPL values obtained using LPM, DPM, ESPI, and AM of the two types of diaphragm are discussed in the following section.

#### 3.1. LPM

For circular diaphragms (30 mm radius), LPM was used for the measurement of displacement amplitude  $A_c$  at the center, and the prediction of SPL at  $r_z=0.1$  (m). The scanning time was very rapid (within 1 min). Normally, without the placement of acoustic meshes on the plates for additional damping, the frequency response associated with displacement amplitude (solid line) on a logarithmic scale results in numerous jagged peaks, as shown in Fig. 10(a). For the first three jagged peaks, the measured displacement amplitudes were 209.59, 5.73, and 3.10  $\mu\text{m}$  at 273, 1000, and 1941 Hz, respectively. In the case of symmetric vibrations (i.e.,  $m=0$ ) in the circular diaphragm using the solution based on the Helmholtz equation in Eq. (7), we were able to determine the first three symmetric modes from the jagged peaks of the resonant frequencies in the frequency-response curves. We then modeled the displacement amplitudes  $z_{0n}(r, f)_{\text{cir}}$  ( $n=1-3$ ) for the entire diaphragm using Eq. (8), as shown in Fig. 11(a).

Using the Rayleigh integral of Eq. (14), we can calculate the SPL curve (dashed line) of modes (0,1)–(0,3), as shown in Fig. 10(a). Clearly, the absolute maximum displacement amplitude (first peak) at 273 Hz, from which we predicted an SPL of 93.9 dB, corresponds to the fundamental resonant frequency and mode (0,1). Similarly, the local maximum displacement amplitudes at 1000 Hz and 1941 Hz, from which we predicted SPLs of 74.1 dB and 74.4 dB, correspond to modes (0,2) and (0,3), respectively. However, the displacement amplitude gradually decreased with an increase in frequency above the frequencies of mode (0,3), and then the jagged peaks of those higher resonant frequencies were not obvious. The phenomenon also represented in Streng's calculation of circular membranes [11]. The predicted SPL will cease to mode (0,3) due to the lack of a significant peak in the displacement amplitude at higher frequencies.

In the case of the annular diaphragm (30 mm outer and 3 mm inner radius), under the same conditions, we measured the displacement amplitude  $A_s$  at  $r=8$  mm [i.e., in the vicinity between the maximum displacements of modes (0,2) and (0,3)], which is determined by normalized displacement as shown in Fig. 5(c). The frequency response curve (solid line) in Fig. 10(b) shows that the first three jagged peaks associated with measured displacement amplitudes of 57.49, 3.02 and 1.20  $\mu\text{m}$  were obtained at 385, 1235 and 2182 Hz, respectively. Similarly with the plot of circular diaphragm, in the case of

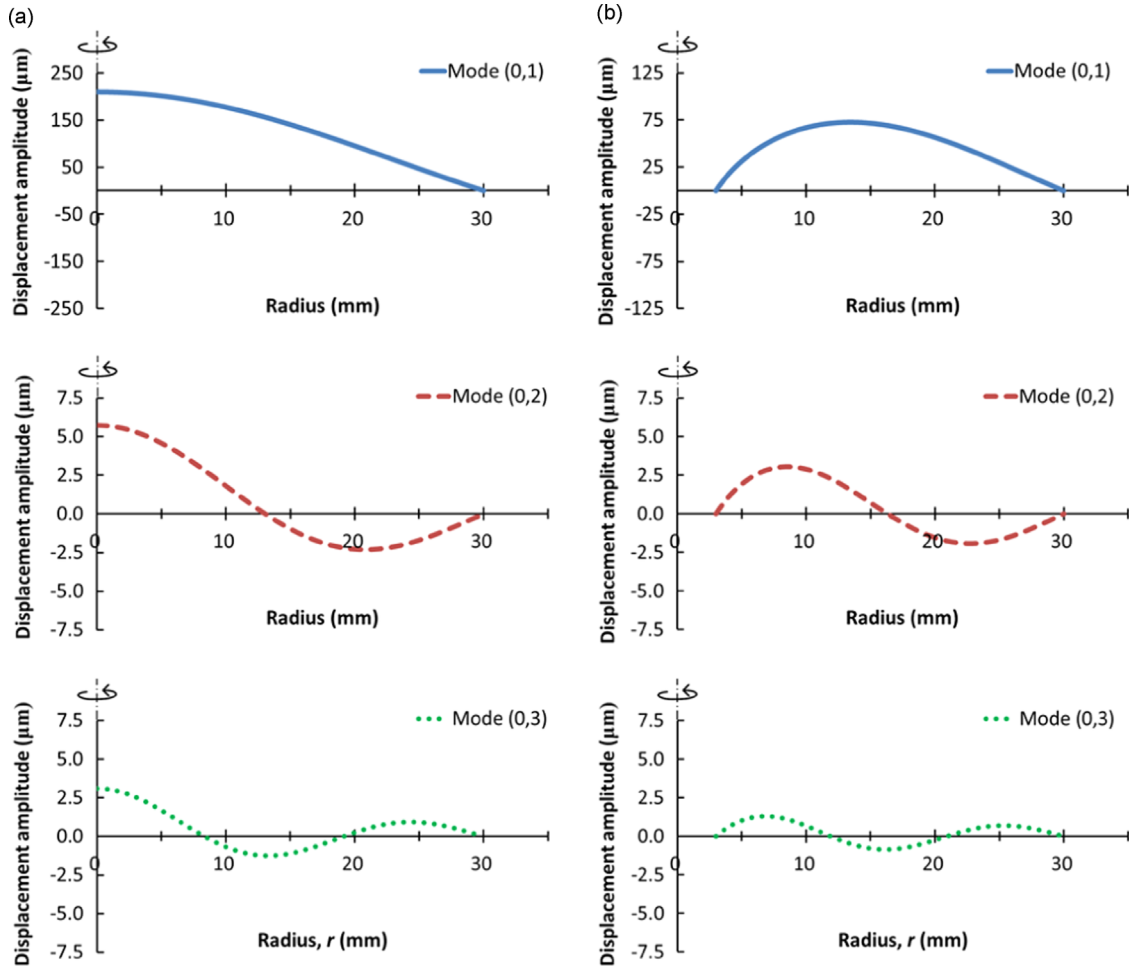


**Fig. 11.** Predicted displacement amplitudes of modes (0,1)–(0,3) obtained using LPM: (a) circular diaphragm with measurement point at  $r=0$ , and (b) annular diaphragm with measurement point at  $r=8$  mm.

symmetric vibrations (i.e.,  $m=0$ ) of the annular diaphragm, the first three symmetric modes are determined at  $r=8$  mm and then modeled the displacement amplitudes  $z_{0n}(r, f)_{\text{ann}}$  ( $n=1-3$ ) in the annular diaphragm using Eq. (12), as shown in Fig. 11(b). Conversely, when measuring the displacement amplitude  $A_s$  at  $r=16.5$  mm [i.e., in the vicinity of maximum displacement of mode (0,1)], the first peak of the displacement amplitude curve (dotted line) was  $101.86 \mu\text{m}$  at 385 Hz. The displacement amplitudes associated with other modes did not achieve significant amplitudes, as shown in Fig. 10(b). In other words, the displacement amplitude of modes (0,2) and (0,3) are relatively small at  $r=16.5$  mm, as shown in Fig. 5(b). The vicinity of central position of the annular diaphragm is only good for mode (0, 1). The determination is difficult for the effective amplitude for modes (0,2) and (0,3), because the displacement is not representative enough to be calculated by LPM.

The Rayleigh integral was used to calculate the SPL curve (dashed line) in Fig. 10(b) for modes (0,1)–(0,3) at  $r=8$  mm. The displacement amplitudes of modes (0,1)–(0,3) at 385, 1235 and 2182 Hz predicted SPLs of 92.2, 71.0, and 75.2 dB, respectively. Hence, selecting an appropriate value of  $r$  is necessary to obtain accurate results in the prediction of SPLs.

In Fig. 10, the mode (0, 1) was used to predict the SPL of an entire piston-like diaphragm. At frequencies above mode (0, 1), the lowest SPL appeared at a break-up frequency ( $f_{\text{bk}}$ ), as shown  $f_{\text{bk}}=583$  Hz in the circular diaphragm or  $f_{\text{bk}}=882$  Hz in the annular diaphragm. Hence, the mode (0, 1) is limited by the break-up frequency. As the frequency increases, an anti-phase component will appear on the vibrating diaphragm which will reduce sound pressure [16]. In predicting the sound radiation from a dynamic speaker driver, the diaphragm is commonly modeled as a flat-piston motion (e.g., the first symmetric mode in circular diaphragm) at a low-frequency range [23]. The flat-piston approximation fails at break-up frequency. In this study, LPM was able to predict the first three modes and SPLs, thereby demonstrating its practicality in the rapid analysis of electrostatic speakers with circular or annular diaphragms at low and mid frequencies.

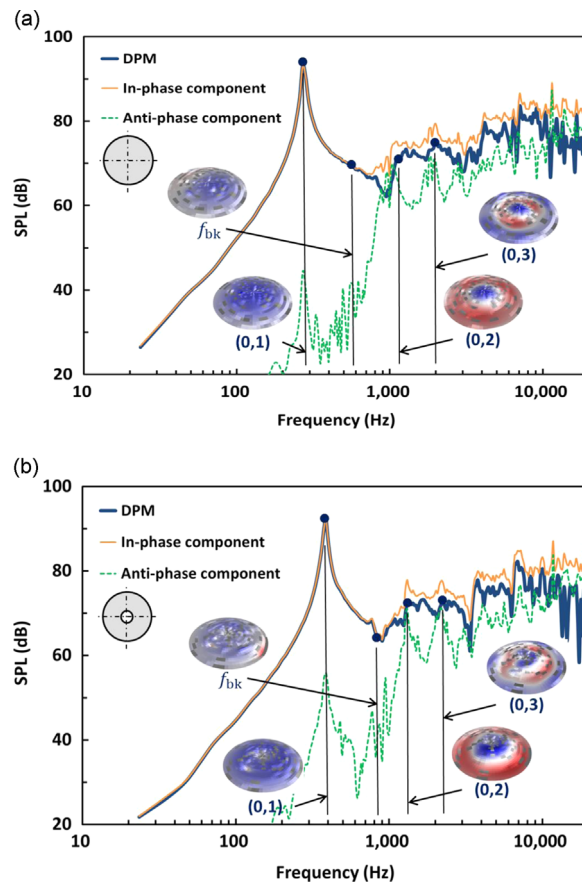


**Fig. 12.** SPL curves obtained using DPM: electrostatic speakers with (a) circular diaphragm (b) annular diaphragm. (For interpretation of the references to color in this figure, the reader is referred to the web version of this article.)

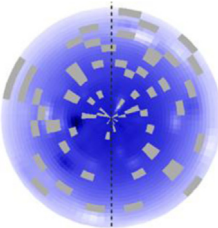
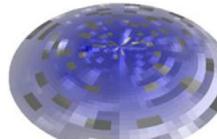
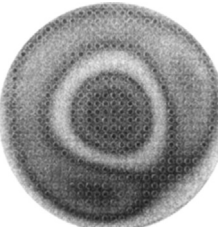
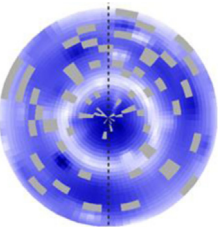
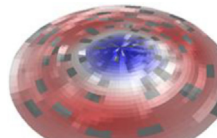
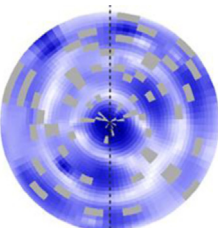
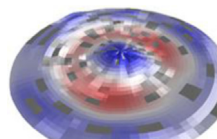
### 3.2. DPM

DPM was used to measure the displacement amplitude values across the entire circular diaphragm, and predict the SPL values from 20 Hz to 20 kHz in the half-space sound field. Vibration analysis was performed using 451 scanning points across the diaphragm, as shown in Fig. 7. A total of 2.5 h was required for the measurement of displacement amplitude in the circular diaphragm. We were unable to obtain measurements at 54 points (as indicated in gray in the following mode shapes determined by DPM). These points were subsequently repaired using SCN analysis software in order to obtain full-field displacement distribution. Fig. 12(a) illustrates that the fundamental resonant frequency at 270 Hz predicts an SPL of 93.1 dB corresponding to mode (0,1). The Predicted SPL values of modes (0,2) and (0,3) at 1160 Hz and 1980 Hz were 71.1 dB and 75.4 dB, respectively. The vibrating mode below the measured break-up frequency ( $f_{bk}$ ) of 586 Hz is indicated by the SPL curve, which is identical to the in-phase component obtained using DPM measurement. The anti-phase component can be disregarded and the in-phase component can be shown to produce the highest SPL. The circular diaphragm at the break-up frequency  $f_{bk}$  cannot slightly be excited on perfect piston motion. Above the break-up frequency, the anti-phase component increases rapidly leading to an obvious drop in the sound pressure. The SPL values of modes (0,2) and (0,3) are certainly shown to be less than the in-phase component of both modes.

Under the same conditions as those used for the annular diaphragm, a total of 2.5 h was required to measure the vibration displacement. Failures at 52 points were repaired using SCN software in order to obtain the full-field displacement distribution. From Fig. 12(b), the predicted SPL values of modes (0,1)–(0,3) at 387, 1313 and 2227 Hz were 92.4, 72.6 and 72.7 dB, respectively. Fig. 12(b) shows that the break-up frequency  $f_{bk}$  occurs at a frequency of 844 Hz. In addition, the 3D view of mode shapes (0,1)–(0,3) of the circular and annular diaphragms using the SCN Analysis Software shows displacement amplitudes and phases (red color vibrates 180° out of phase with blue color), and nodal circles (white color) from Fig. 12. The measured mode shapes (0,1)–(0,3) in DPM are in good agreement with the predicted modes (0,1)–(0,3) in LPM (see Fig. 11). Despite the fact that 12% of the points had to be repaired to obtain the mode shapes of the circular and annular diaphragms, the DPM revealed a relationship between vibrational and acoustic frequency-response characteristics from 20 Hz to 20 kHz using the SCN of KLIPPEL.

**Table 2**

Mode shapes, resonant frequencies, and applied voltages associated with modes (0,1)–(0,3) from electrostatic speaker with circular diaphragm obtained using ESPI and DPM.

Mode information	ESPI	DPM	
		2D view	3D view
(0, 1)	Mode shape		 
	Frequency, Hz Applied voltage, V <sub>rms</sub>	269 1.77	270 100
(0, 2)	Mode shape		 
	Frequency, Hz Applied voltage, V <sub>rms</sub>	1116 9.25	1160 100
(0, 3)	Mode shape		 
	Frequency, Hz Applied voltage, V <sub>rms</sub>	1980 31.82	1980 100

### 3.3. ESPI

Tables 2 and 3 present the mode shapes, resonant frequencies, and applied voltages obtained from the ESPI and DPM results for the first three mode shapes of the electrostatic speakers with circular and annular diaphragms. The nodal circles are the brightest region in the mode shapes obtained using ESPI. The other white and dark fringes indicate contours associated with constant vibrating displacement. The corresponding magnitude of each fringe is described in Section 2.4. Errors in DPM measurement can be detected and repaired using SCN analysis software, in which repaired points are highlighted in gray. In 2D images, displacement amplitudes are represented by the intensity of the blue color. In 3D images, convex (positive) and concave (negative) displacements are represented using blue and red, respectively. Thus, the nodal circles and fringe patterns obtained from ESPI results can be verified by comparing the mode shapes with DPM results. After observing each mode shape in the number of nodal circles, the ESPI measurement agrees fairly well with the DPM in resonance.

Based on the assumption of linear operation, the displacement amplitude can be calculated using the applied voltage obtained from ESPI measurement. For example, mode shape (0,2) at the center of the circular diaphragm (see Table 2) is evaluated using dark fringe,  $i=3$ , where the displacement amplitude ( $A_3$ ) is  $0.446 \mu\text{m}$  (see Section 2.4) using an applied voltage of  $9.25 \text{ V}_{\text{rms}}$ . Thus, the displacement amplitude at  $100 \text{ V}_{\text{rms}}$  is approximately  $4.82 \mu\text{m}$ ; i.e.,  $0.446 \mu\text{m} \times (100/9.25) = 4.82 \mu\text{m}$ . This result is close to the measured displacement amplitude of  $5.73 \mu\text{m}$  at  $100 \text{ V}_{\text{rms}}$  using LPM [see Fig. 10(a)]. Despite relatively low exciting voltages in ESPI and a large number of repaired points in DPM, mode shapes, resonant frequencies and applied voltages obtained by the ESPI and DPM can be determined consistently with the quantitative displacement amplitudes.

**Table 3**

Mode shapes, resonant frequencies, and applied voltages associated with modes (0,1)–(0,3) from electrostatic speaker with annular diaphragm obtained using ESPI and DPM.

Mode information	ESPI	DPM	
		2D view	3D view
(0, 1)	Mode shape		
	Frequency, Hz Applied voltage, V <sub>rms</sub> Mode shape	390 1.77	387 100
(0, 2)			
	Frequency, Hz Applied voltage, V <sub>rms</sub> Mode shape	1165 3.01	1313 100
(0, 3)			
	Frequency, Hz Applied voltage, V <sub>rms</sub>	2258 15.91	2227 100

### 3.4. AM

Electrostatic speakers with circular or annular diaphragms were fixed to a baffle in an anechoic chamber to measure the SPL curves from 20 Hz to 20 kHz. We compared the SPL curves obtained using LPM, DPM, and AM in order to study the relationship between predicted and measured values associated with acoustic frequency-response characteristics.

Fig. 13(a) presents the AM results of the circular diaphragm, in which the fundamental resonant frequency corresponds to the mode (0,1) with a measured SPL of 87.6 dB at 280 Hz (i.e., the first peak in the frequency spectrum). The predicted SPL values of mode (0,1) in LPM and DPM are close to the measured SPL values of mode (0,1) in AM, particularly below the break-up frequency. At mid-frequency band, the SPL values of modes (0,2) and (0,3) predicted using LPM are also consistent with AM results. Table 4 summarizes the AM, LPM and DPM results with regard to SPLs and the frequencies associated with modes (0,1)–(0,3). As shown in Fig. 13(b), we also measured the SPL curves of annular diaphragms from 20 Hz to 20 kHz. Modes (0,1)–(0,3) measured 87.0, 72.5, and 73.4 dB at frequencies of 375, 1250, and 2120 Hz, respectively. Table 5 summarizes the results obtained using AM, LPM, and DPM.

In Fig. 14, Each SPL value of modes (0,1)–(0,3) with the annular diaphragm is respectively close to that the circular diaphragm; however, the resonant frequencies of modes (0,1)–(0,3) obtained from the annular diaphragm are higher than those from the circular diaphragm, respectively. Below 60 Hz, a number of peaks were observed in the SPL curves of both diaphragms due to background noise in the anechoic chamber. Above 6 kHz, the SPL gradually decreases with an increase in frequency. Some of our measured results contradict the expectations of fluid-structure coupling theory [11,12]. The decay in SPL may be due to losses in the driving amplifier or a near-field effect. Although the SPLs are affected by the measured background noise below 60 Hz and decay above 6 kHz, they have no effect on investigating vibrational modes and sound radiation of both circular and annular diaphragms using the four evaluation methods, i.e. LPM, DPM, ESPI and AM.

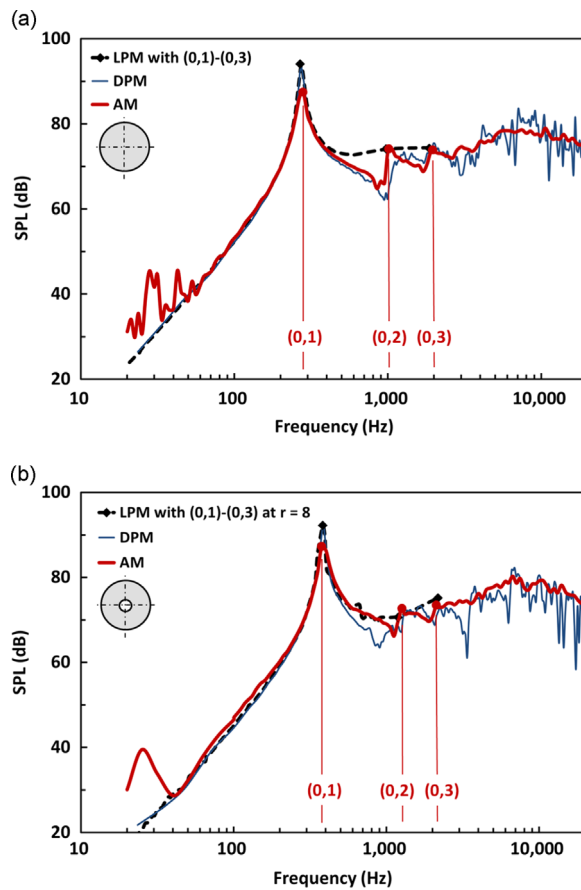


**Fig. 13.** SPL curves obtained using LPM, DPM, and AM: electrostatic speakers with (a) circular diaphragm and (b) annular diaphragm.

**Table 4**

SPLs and resonant frequencies associated with modes (0,1)–(0,3) from electrostatic speaker with circular diaphragm obtained using AM, LPM, and DPM.

Mode ( $m,n$ )	Parameters	AM	LPM (error to AM, %)	DPM (error to AM, %)
(0,1)	SPL, dB	87.6	93.9 (7.19)	93.1 (6.28)
	Frequency, Hz	280	273 (-2.50)	270 (-3.57)
(0,2)	SPL, dB	74.1	74.1 (0.00)	71.1 (-4.05)
	Frequency, Hz	1060	1000 (-5.66)	1160 (9.43)
(0,3)	SPL, dB	73.4	74.4 (1.36)	75.4 (2.72)
	Frequency, Hz	2000	1941 (-2.95)	1980 (-1.00)

**Table 5**

SPLs and resonant frequencies associated with modes (0,1)–(0,3) from electrostatic speaker with annular diaphragm obtained using AM, LPM, and DPM.

Mode ( $m,n$ )	Parameters	AM	LPM (error to AM, %)	DPM (error to AM, %)
(0,1)	SPL, dB	87.0	92.2 (5.98)	92.4 (6.21)
	Frequency, Hz	375	385 (2.67)	387 (3.20)
(0,2)	SPL, dB	72.5	71.0 (-2.07)	72.6 (0.14)
	Frequency, Hz	1250	1235 (-1.20)	1313 (5.04)
(0,3)	SPL, dB	73.4	75.2 (2.45)	72.7 (-0.95)
	Frequency, Hz	2120	2182 (2.92)	2227 (5.05)

Tables 2–5 list the predictions based on LPM and DPM with regard to SPL values of the first three symmetric mode shapes. These values for circular and annular diaphragms are in strong agreement with the results obtained using AM. Furthermore, these results are sufficiently stable to estimate the SPL values in the low- and mid-frequency bands. This demonstrates that these four measurement methods can be used for the analysis and diagnostics of electrostatic speaker systems. The pros and cons of each method are summarized in Table 6. For example, LPM would be an ideal solution when

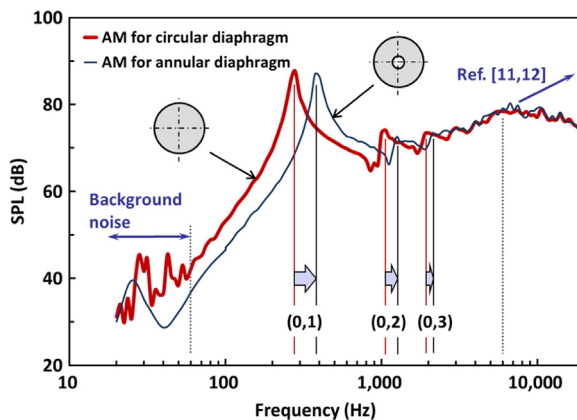


**Fig. 14.** SPL curves obtained using AM: electrostatic speakers with circular diaphragm and annular diaphragm.

**Table 6**

Summary of properties of LPM, DPM, AF-ESPI and AM.

Property	Measurement method			
	LPM	DPM	AF-ESPI	AM
Measured District	One point	Multipoints (451 pts)	One surface	One surface
Measured Time	Rapid ( $< 1$ min)	Slow (About 2.5 h)	Slow (About 30 min)	Rapid ( $< 1$ min)
Measured Field	Vibrational	Vibrational	Vibrational	Acoustic
Measured Frequency	Low to Mid	Audible Band (20 Hz to 20 kHz)	Specified Modes	Audible Band (20 Hz to 20 kHz)
Application	On-line detection	R&D	R&D	On-line detection

measuring the SPLs of speaker drivers in situations (e.g., on-line detection) with environmental noise. The LPM is a measurement of vibrational field and prediction of sound pressure without worrying about the effect of environmental noise. Furthermore, the use of LPM, DPM, and ESPI can lead to novel insights with regard to the vibrational mode and sound radiation behaviors of electrostatic speakers based on ITO plates.

#### 4. Conclusions

This study used transparent ITO plates to measure the vibrational mode of circular and annular diaphragms using a laser system, in order to predict the SPLs using Helmholtz and Rayleigh integral equations. Traditional acoustic measurements (AMs) were used to evaluate the predictions made using LPM results in the low- and mid-frequency bands as well as DPM results from 20 Hz to 20 kHz. The SPL curves predicted by LPM and DPM are in good agreement with the results obtained using AM, as shown in Tables 4 and 5. LPM proved particularly adept at quickly and accurately predicting SPLs from the displacement amplitudes of the first three symmetric modes. Based on the assumption of linear operations, the DPM and ESPI techniques determine the visualization of mode shapes (0,1)–(0,3); and the ESPI can evaluate the displacement amplitude for electrostatic speakers.

Under the same measurement conditions, electrostatic speakers with a push–pull configuration present similarly jagged peaks in the SPL curves, regardless of whether a circular or annular diaphragm is employed. The resonant frequency of each mode obtained from the annular diaphragm is slightly higher than that obtained from a circular diaphragm. The first three symmetric modes are measured and predicted to give accurately qualitative and quantitative results in their SPL curves. This paper proposes an efficient and accurate means of measuring vibration and sound radiation. A further study will be done on applying piezoelectric and electret speakers.

#### Acknowledgments

The authors gratefully acknowledge financial support for this research provided by the Ministry of Science and Technology, Taiwan, Republic of China, under Grant MOST104-2628-E-011-002-MY3. We would also like to give special thanks to the National Taiwan University of Science and Technology for providing financial and research support (105H4218).

## References

- [1] W.T. Selsted, The electrostatic earphone, *Journal of the Audio Engineering Society* 9 (1961) 145–147.
- [2] J. Borwick, *Loudspeaker and Headphone Handbook*, 3rd ed. Focal Press, Oxford, 2001, 108–195.
- [3] R.R. Sanders, *The Electrostatic Loudspeaker Design Cookbook*, 1st ed. Audio Amateur Press, New Hampshire, 1995, 11–14.
- [4] J.P. Wilson, High-quality electrostatic headphones, *Wireless World* (1968) 440–443.
- [5] P.D. Harvey, Electrostatic headphone design, *Wireless World* (1971) 527–531.
- [6] N. Pollock, Electrostatic headphones, *Wireless World* (1979) 51–55.
- [7] P.M. Morse, *Vibration and Sound*, 2nd ed. McGraw-Hill, New York, 1948, 172–216.
- [8] G.R. Sharp, Finite transform solution of the symmetrically vibrating annular membrane, *Journal of Sound and Vibration* 5 (1) (1967) 1–8.
- [9] M. Jabareen, M. Eisenberger, Free vibrations of non-homogeneous circular and annular membranes, *Journal of Sound and Vibration* 240 (3) (2001) 409–429.
- [10] J.H. Streng, Calculation of the surface pressure on a vibrating circular stretched membrane in free space, *Journal of the Acoustical Society of America* 82 (2) (1987) 679–686.
- [11] J.H. Streng, Sound radiation from a circular stretched membrane in free space, *Journal of the Acoustical Society of America* 37 (3) (1989) 107–118.
- [12] T.J. Mellow, L.M. Kärkkäinen, On the sound field of a membrane in free space and an infinite baffle, *Journal of the Acoustical Society of America* 120 (5) (2006) 2460–2477.
- [13] M.R. Bai, R.L. Chen, C.J. Wang, Electroacoustic analysis of an electret loudspeaker using combined finite-element and lumped-parameter models, *Journal of the Acoustical Society of America* 125 (6) (2009) 3632–3640.
- [14] M.R. Bai, Chun-Jen Wang, Dar-Ming Chiang, Shu-Ru Lin, Experimental modeling and design optimization of push–pull electret loudspeakers, *Journal of the Acoustical Society of America* 127 (4) (2010) 2274–2281.
- [15] Q. Zhou, A. Zettl, Electrostatic graphene loudspeaker, *Applied Physics Letters* 102 (2013) 223109.
- [16] H.Y. Chiang, Y.H. Huang, Vibration and sound radiation of an electrostatic speaker based on circular diaphragm, *Journal of the Acoustical Society of America* 137 (4) (2015) 1714–1721.
- [17] Y.H. Huang, C.C. Ma, Z.Z. Li, Investigations on vibration characteristics of two-layered piezoceramic disks, *International Journal of Solids and Structures* 51 (1) (2014) 227–251.
- [18] A.W. Leissa, M.S. Qatu, *Vibration of Continuous Systems*, McGraw-Hill, New York, 2011, 181–220.
- [19] A.D. Pierce, *Acoustics: An Introduction to its Physical Principles and Applications*, McGraw-Hill, New York, 1981, 208–249.
- [20] F. Fahy, P. Gardonio, *Sound and Structural Vibration: Radiation, Transmission And Response*, 2nd ed. Academic Press, London, 2007, 135–241.
- [21] W. Klippel, J. Schlechter, Distributed mechanical parameters of loudspeakers Part 1: measurements, *Journal of the Acoustical Society of America* 57 (7/8) (2009) 500–511.
- [22] Y.H. Huang, C.C. Ma, Experimental and numerical investigations of vibration characteristics for parallel-type and series-type triple-layered piezoceramic bimorphs, *IEEE Transactions on Ultrasonics, Ferroelectrics, and Frequency Control* 56 (12) (2009) 2598–2611.
- [23] W.M. Leach, Jr., *Introduction to Electroacoustics and Audio Amplifier Design*, 4th ed. Kendall Hunt Pub, Co, Iowa, 2010, 1–14.